Large-Scale Roll-to-Roll Fabrication of Vertically Oriented Block Copolymer Thin Films

Gurpreet Singh,[†] Saurabh Batra,[†] Ren Zhang,[†] Hongyi Yuan,[†] Kevin G. Yager,[‡] Miko Cakmak,[†] Brian Berry,[§] and Alamgir Karim[†,*]

[†]Department of Polymer Engineering, The University of Akron, Akron, Ohio 44325, United States, [‡]Center for Functional Nanomaterials, Brookhaven National Laboratory, Upton, New York 11973, United States, and [§]Department of Chemistry, University of Arkansas at Little Rock, Little Rock, Arkansas 72204, United States

ABSTRACT Large-scale roll-to-roll (R2R) fabrication of vertically oriented nanostructures *via* directed self-assembly of cylindrical block copolymer (c-BCP) thin films is reported. Nearly 100% vertical orientation of cylinders in sub-100 nm c-BCP films under optimized processing *via* a dynamic sharp temperature gradient field termed Cold Zone Annealing-Sharp or `CZA-S' is achieved, with successful scale-up on a prototype custom-built 70 ft × 1 ft R2R platform moving at 25 μm/s, with 9 consecutive CZA units. Static thermal annealing of identical films in a conventional vacuum oven fails to produce comparable results. As a potential for applications, we fabricate high-density silicon oxide nanodot arrays from the CZA-S annealed BCP thin film template.

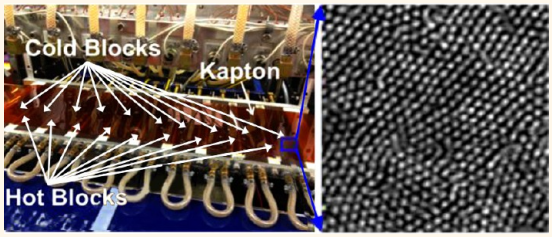

KEYWORDS: directed self assembly · block copolymer · roll to roll · zone annealing

Block copolymer (BCP) thin films remain heavily researched by academia and industry due to their potential applications in future generations of high-tech devices. The most exciting and sought-after BCP property is their self-assembly into a diversity of periodic nanostructures with sizes in the range of 5−100 nm.[1−8] These periodic nanostructures have found use in a wide spectrum of applications such as nanolithography,[9−11] photonics,[12,13] plasmonics,[14] sensors,[15,16] storage media,[17] membranes,[18] drug delivery,[19] cell culture,[20] mesoporous carbons,[21] *etc.*[3−7] The critical requirement for these applications is the fabrication of well-ordered BCP nanostructures that are oriented either horizontally or vertically with respect to the substrate. After significant effort over the past decade, several techniques are now available to direct BCP self-assembly for highly ordered nanostructures.[8,22−32] The present BCP directed self-assembly (DSA) efforts are focused toward enhanced self-assembly kinetics and fabrication of high aspect-ratio nanostructures. In this regard, recently, solvent and "solvothermal" based BCP-DSA techniques in conjunction with graphoepitaxy are shown to be effective.[29,30,33,34] However, most BCP-DSA methods are generically applicable only over small areas and batch operations. Additionally, solvent-based BCP-DSA methods are not the most attractive since they may use hazardous solvents, require sophisticated infrastructure and are incompatible with many flexible substrates that are generally organic in composition. On the other hand, a dynamic thermal field based technique known as zone annealing or zone refining is a simple and universally applicable continuous roll-to-roll (R2R) process that has gained increasing importance as a BCP-DSA method for rapidly tuning the orientation of BCP nanostructures.[34−40] The concept of zone annealing (ZA) originated in the metallurgy and semiconductor industry[41] with the essential idea to restrict the crystal grain growth to a narrow melt zone that acts like a crystal-refining region. Lovinger *et al.*[42] observed that ZA of semicrystalline polymers led to oriented single crystals along ZA direction over macroscopic scales. Depending on whether the maximum temperature (T_{MAX}) of the temperature gradient (∇T) curve is above or below the BCP order−disorder transition temperature

* Address correspondence to alamgir@uakron.edu.

Received for review March 4, 2013 and accepted May 6, 2013.

Published online May 06, 2013
10.1021/nn401094s

`$T_{ODT}$', BCP-ZA is classified as hot zone annealing[35,36] or cold zone annealing[37−40,43] `CZA', respectively. Previously, we observed that a broad ∇T field strength leads to long-range ordering of horizontally oriented cylinders whereas a sharp ∇T field strength (referred to as CZA-S) preferentially produces hexagonally close-packed vertically oriented BCP cylinders in the 100−1000 nm thickness limit.[39] Recently, we also developed a novel modification of the CZA-S process where we coupled the dynamic thermal field with an induced soft-shear field that rapidly (12 mm/min) yielded highly oriented and hierarchically patternable horizontal BCP cylinders.[40] Here we emphasize the large-scale continuous fabrication of vertically oriented sub-100 nm thick BCP thin films *via* a dynamic thermal field process by exploiting synergy of processing dynamics with finite size effects of BCP thin film behavior. Our focus here is to demonstrate the scalability of this process up to industrial-scale, and for the first time we display successful scale-up on a 70 ft × 1 ft (length × width) custom-built R2R platform with 9 consecutive cold-hot-cold zones. It is worthy to mention that there are a few other reports[44] of R2R processes for DSA of BCPs that are highly specific to liquid crystal BCPs only. Importantly, the R2R CZA-S process we develop here is free of any physical or chemical templates, which minimizes the number of processing steps that is important from an industrial-scale application point-of-view. To highlight the functional nature of these films and potential for a range of applications as discussed before, we demonstrate their etchability and use as templates for fabricating high-density arrays of silicon oxide nanodots.

RESULTS AND DISCUSSION

Figure 1 shows the schematic of the CZA-S process, the temperature gradient curve, the residence glass transition to glass transition `$T_g$ to $T_g$' time of the poly(styrene-*block*-methylmethacrylate) `PS-PMMA' thin film at various annealing velocities, and morphology of the PS-PMMA thin film, CZA-S annealed at different velocities. Previously, we observed that CZA-S annealing of the sub-100 nm BCP films formed terraced structures or islands that led to either

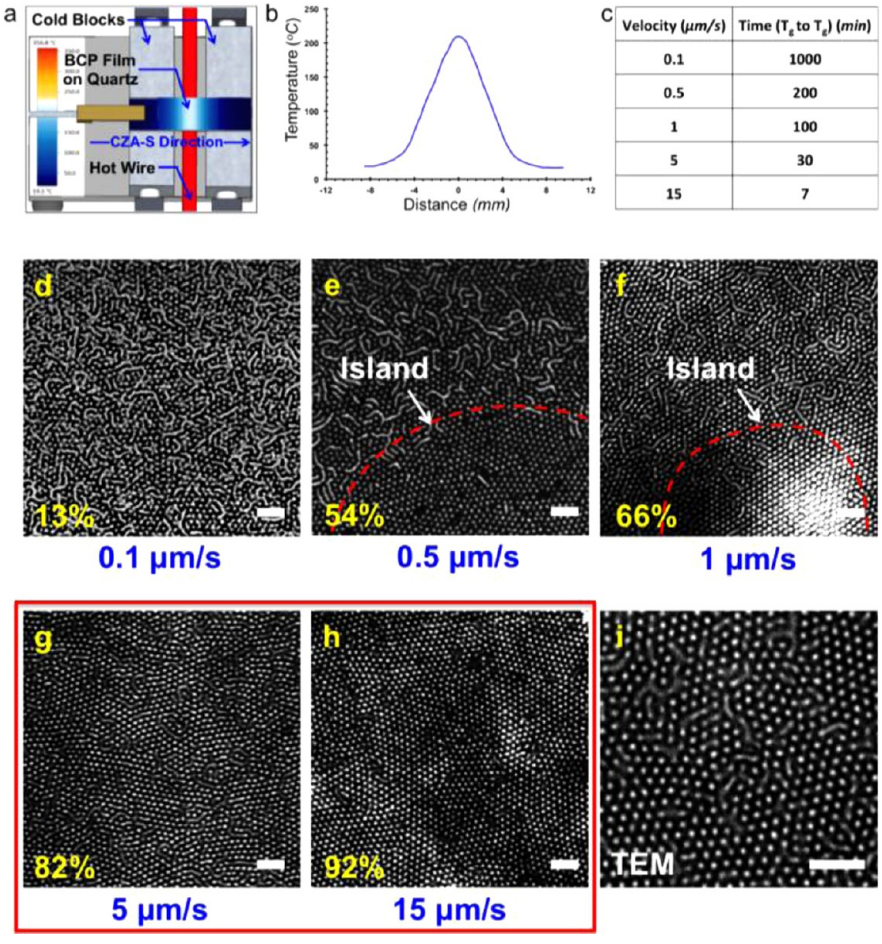

Figure 1. CZA-S process dynamics and its effect on BCP morphology. (a) Schematic of the CZA-S apparatus. (b) Temperature gradient curve. (c) Conversion of CZA-S annealing speed to the T_g to T_g residence time for PS-PMMA thin film. (d−h) AFM morphology of PS-PMMA thin film annealed at 0.1, 0.5, 1, 5, and 15 μm/s, respectively. Insets also show the %vertical cylinder population for corresponding images. (i) TEM image of PS-PMMA film CZA-S annealed at 15 μm/s at random location. Size of scale bar is 200 nm.

horizontally oriented cylinders or mixed morphology of vertically and horizontally oriented cylinders.[39] Here we show that by tuning the CZA-S parameters to restrict the island formation, we can induce *ca.* 95% hexagonally close packed vertical cylinders in the sub-100 nm (approximately 1.7 L_0 or 75 nm, L_0 is the domain spacing) BCP film thickness regime.

As shown in Figure 1a, PS-PMMA thin film is flow-coated[45] on the quartz substrate that is translated across a temperature gradient generated by the hot wire surrounded with the cold blocks. As the sample is translated across the cold-hot-cold region, the BCP thin film experiences a temperature profile as shown in Figure 1b. The maximum temperature (T_{MAX}) and the maximum temperature gradient (∇T_{MAX}) are 210 and 45 °C/mm, respectively. The BCP thin films are CZA-S annealed at different velocities, which is inversely correlated to their T_g to T_g residence time or effective annealing time as shown in Figure 1c. Figure 1d−h show the evolution of the PS-PMMA thin film morphologies imaged by an atomic force microscope (AFM), that are CZA-S annealed at different velocities. AFM images showing PS-PMMA morphology at higher CZA-S velocities are shown in Supporting Information, Figure S1. The PS-PMMA thin films annealed at 0.1, 0.5, and 1 μm/s spend 1000, 200, and 100 min, respectively, above the BCP's T_g (Figure 1d−f). The insets of Figure 1d−f shows arrows pointing toward the terraced structures or islands that typically develop in the cylindrical BCP thin films of incommensurate ($nL_0 < h < (n + 1/2)L_0$) film thickness.[3] The phenomena of terrace formation in cylinder forming block copolymer thin films has already been studied in detail.[3] For the ease of understanding, here we provide a brief summary of the phenomena. The as-cast BCP thin film morphology exhibits disordered microstructure since the fast solvent evaporation during flow coating does not leave enough time for microphase separation. As the BCP thin film is supplied with sufficient thermal energy during CZA-S annealing, the BCP chains become mobile and the PMMA phase tries to progressively wet the substrate−film interface due to stronger attraction of PMMA and SiO_2 compared to PS and SiO_2. The PS block on the other hand progressively tries to wet the air−film interface since the surface energy of PS is slightly less than that of PMMA. As the initial film thickness is incommensurate, the BCP chains have to stretch and compress to accommodate these BCP wetting characteristics. In order to avoid excessive stretching/compression of the BCP chains, the BCP thin film forms terraced structures as has been observed by Kim *et al.*[46] However, at shorter time intervals (*i.e.* high CZA-S annealing velocity) where PMMA and PS have not yet wetted the substrate surface and the air surface, respectively, BCP thin film can avoid the chain stretching and compression by adopting vertical orientation that can "commensurably" accommodate any thickness, as seen in Figure 1g,h. With progressing time, PMMA wets the substrate surface whereas PS wets the air surface that also leads to the formation of terrace structures as seen in Figure 1d−f. The insets of Figure 1d−f also show the %vertical cylinder population that decays sharply with the decreasing CZA-S annealing velocity or with the increasing T_g to T_g residence time. In short, when the PS-PMMA thin films are CZA-S annealed at velocities of 1 μm/s and less, they develop terraced structures that lead to poor cylinder orientation. The polymer mass flow, from the lower thickness region to the higher thickness region, associated with terracing of the thin film causes the disruption of the BCP morphology.[46] On the other hand, the BCP thin films annealed at 5 and 15 μm/s spend just 30 and 7 min, above the PS-PMMA T_g, respectively, and the corresponding morphology developed in Figure 1g,h indicates that the terracing of the BCP thin film is kinetically hindered with predominantly hexagonally close packed vertically oriented cylinders. We have thus demonstrated that the CZA-S parameters can be tuned for continuous fabrication of hexagonally close packed vertically oriented cylinders (Figure 1h) even in the nanotechnologically attractive sub-100 nm film thickness regime. It is important to note that previously,[39] BCP films thicker than 100 nm showed disordered morphology when CZA-S annealed at 15 μm/s. The transmission electron microscopy (TEM) image, shown in Figure 1i, of the PS-PMMA thin film that was CZA-S annealed at 15 μm/s reveals the through-film morphology. TEM measurements were taken on an average of 3 samples and at 3 different locations for each sample (see Supporting Information Figure S2 for additional TEM images of the CZA-S annealed BCP thin films). The majority of the area exhibit hexagonally close packed vertically oriented cylinders, however at certain areas, underlying short horizontal cylinders can be seen. It is important to observe that the color-intensity of the horizontally oriented cylinders in Figure 1i is lower than the color-intensity of vertically oriented cylinders and the horizontal cylinders seem to connect the vertically oriented cylinders together. These observations confirm that the majority of the vertically oriented cylinders persist through the film (also confirmed by GISAXS later), if not the entire film thickness, and the short horizontal cylinders lie below the vertically oriented cylinders.

Comparatively, Figure 2a−e shows the morphology evolution of the 1.7 L_0 thick PS-PMMA thin films that are thermally annealed in a vacuum oven at 210 °C for varying time periods (additional images showing the thin film morphology at different times are in Supporting Information, Figure S3). The inset values in Figure 2a−e show the %vertical cylinder population for the corresponding annealing time is nonmonotonic, peaking between very short time annealing

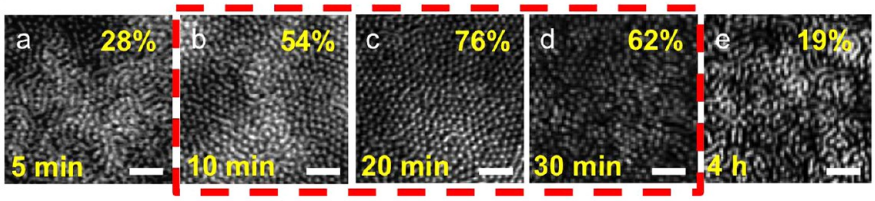

Figure 2. Effect of uniform thermal oven annealing on BCP morphology with time. (a−e) AFM morphology of the 75 nm thick PS-PMMA thin films when thermally annealed in a conventional vacuum oven for 4 h, 30 min, 20 min, 10 min, and 5 min. Insets also show the %vertical cylinder population for corresponding images. Size of scale bar is 200 nm.

and very long time annealing, respectively. Figure 2b−d indicates that there exists a window of opportunity, *i.e.*, an intermediate annealing time where the %vertical population can be maximized (Figure 2c) even in oven annealing without substrate modification, a result that has not been significantly reported previously. This is an important observation that is in agreement with our previous result[39] where we show randomly packed vertically oriented cylinders (65% vertical population for 10 min annealing) at short oven annealing times for 250 nm thick PS-PMMA films. The physical phenomena behind vertical orientation of cylinders in the optimal range of relatively short time annealing is the normal thermal expansion induced chain alignment of BCP cylinders; whereas the isotropic relaxation and surface (air and substrate) wetting of polymer chains in the limit of long time annealing causes loss of vertical orientation, while slow ordering kinetics at very short annealing times does not lead to sufficient ordering.[39,47]

Even though 20 min of thermal annealing in a vacuum oven can lead to 76% vertically oriented cylinders (Figure 2c), the fast Fourier transform (FFT) of the AFM image (Figure 3a) shows a single, broad and diffuse ring indicative of early stage phase separation with random orientation of the cylinders. On the other hand, Figure 3b shows the FFT of the CZA-S annealed BCP thin film AFM image (Figure 1h) that clearly displays a sharp first order ring with surrounding secondary and tertiary rings. The primary, secondary and tertiary rings are spaced in reciprocal space ratio of 1:$\sqrt{3}$:2, respectively, which is characteristic of the hexagonally well-packed vertical cylinders. However, instead of sharp hexagonal spots, a sharp ring is observed (Figure 3b) that indicates a polygrain structure, as seen in Figure 1h. For a more quantitative comparison between the dynamic CZA-S annealing and the static thermal annealing in a vacuum oven, in Figure 3c, we plot the %vertical population of cylinders obtained *via* CZA-S annealing and uniform thermal oven annealing *versus* the effective annealing time. The T_{MAX} during CZA-S process is chosen as the effective temperature and the T_g to T_g residence time is used as the comparative effective annealing time for the uniform thermal annealed thin films.

At this point, it should be noted that the uniform oven annealing conditions are controlled such that the

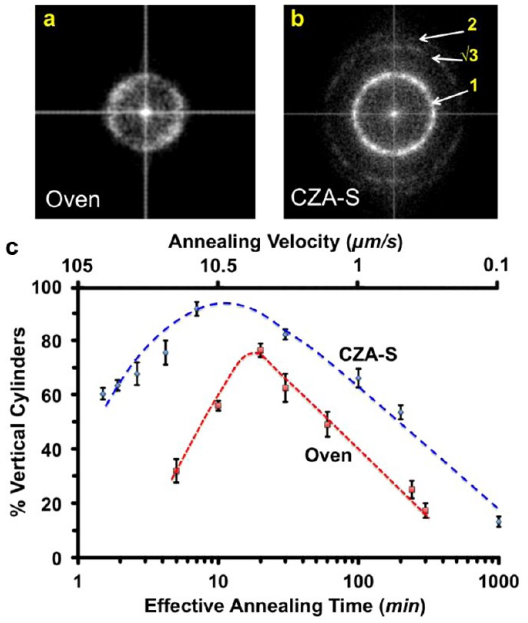

Figure 3. Comparing the effect of dynamic CZA-S annealing and static thermal annealing on BCP morphology. (a) Fast Fourier transform of Figure 2c. (b) Fast Fourier transform of Figure 1h. (c) Plot of %vertical cylinder population *versus* annealing time. The fitted lines are visual aids and are arbitrary in nature.

oven temperature $T \sim$ CZA-S $T_{MAX,}$ and the oven annealing time $t \sim$ CZA T_g to $T_{g,}$ are not statistically equivalent conditions to the CZA-S process. But in fact, these conditions provide uniform oven annealed BCP thin films an undue advantage in terms of temperature and annealing time because in CZA-S, the sample spends only a fraction of total time at T_{MAX} and the CZA-S annealing time near T_g does not lead to any effective ordering. As can be observed from Figure 3c, both the CZA-S annealed and the oven annealed BCP thin films exhibit a nonmonotonic trend. However, CZA-S annealing samples fare significantly better than uniform oven annealing ones for all comparative time scales, and most importantly, the CZA-S annealed thin films peak to as high as 95% vertically oriented cylinders. This fraction is uniform thermal annealing, nor is it possible to obtain hexagonally close packed vertically oriented cylinders *via* uniform oven annealing. Interestingly, the development of vertically oriented cylinders for CZA-S annealing and uniform thermal annealing at extremely short time-scales prior to peaking in %vertical cylinders

differs significantly. The CZA-S annealed thin films show a minimal value of 60% vertical cylinders at time $t = T_g$ to $T_g < 2$ min, whereas the uniform thermally annealed thin films exhibit a minimal value of 20% vertical cylinders at effective annealing time $t = 5$ min. This indicates that the dynamics of the BCP ordering are much more rapid for CZA-S annealing and differ significantly from the usual uniform thermal annealing process. Therefore, from Figure 3, we can conclude that the CZA-S process is much more effective than the conventional thermal oven annealing for fabricating hexagonally well packed vertically oriented cylinders. PS-PMMA BCPs inherently have a low effective χ-parameter that limits the smallest size of nanostructures that can be fabricated *via* DSA of PS-PMMA BCP thin films. For this reason, there is growing emphasis on high effective χ-parameter BCPs so as to achieve sub-15 nm nanostructures.[31,48] One such example is the poly(styrene-*b*-2-vinyl pyridine) (PS-P2VP) BCP system. We observe that the CZA-S process does not vertically orient cylindrical PS-P2VP BCP thin films (see Supporting Information Figure S4). However, it is important to note that this vertical orienting CZA-S process critically depends on the strength of the individual blocks interaction with the substrate. For a BCP system such as PS-P2VP, the P2VP block exhibits an extremely strong interaction with the quartz (silica) substrate surface such that we do not observe vertically oriented cylinders *via* CZA-S annealing. To give an idea about the how strongly P2VP interacts with the substrate in comparison to PMMA, we can look at how the thin film T_g changes for ultrathin films. The ultrathin films of P2VP show an enhanced T_g as high as +40 K compared to its bulk T_g, whereas ultrathin films of PMMA show approximately the same T_g compared to its bulk T_g.[49] By comparison, a BCP system such as poly(styrene-b-lactide) (PS-PLA)[50] has a similar advantage as the PS-P2VP system, *i.e.*, a high effective χ-parameter, yet experiments have demonstrated that the vertical orientation is favored as both blocks have similar surface energies but do not interact strongly with the substrate surface (even lower interaction with silica than the PS-PMMA system). Therefore, we believe that the CZA-S process is not limited only to the length scale of nanostructures that can be obtained *via* DSA of PS-PMMA BCP thin films; in fact it can be utilized to fabricate sub-15 nm nanostructures as well.

Next, toward establishing whether the CZA-S results could be accomplished under realistic manufacturing conditions, we zone annealed PS-PMMA thin films using a unique custom-built roll-to-roll (R2R) machine equipped with 9 sequential CZA units, although the results presented in Figure 4 are for R2R conditions utilizing only a single CZA unit. Figure 4a shows the novel 70 ft × 1 ft custom-built R2R machine (named EMP-1) that was utilized for the large-scale CZA-S experiments.[51] Figure 4b shows the flexible kapton film flow-coated with the 75 nm thick PS-PMMA BCP film placed on top of the 9 sequential CZA units. The dimensions of the PS-PMMA film that was coated on the kapton substrate was 12 in. × 3 in. (length × width).

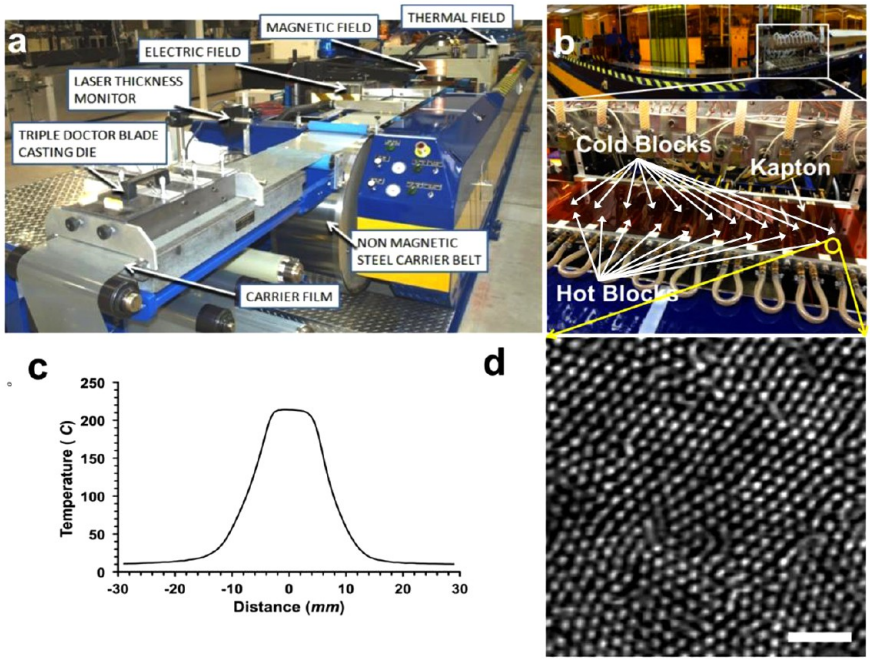

Figure 4. Large-scale R2R fabrication of vertically oriented BCP thin films. (a and b) Images of the custom-built prototype R2R machine with 9 sequential cold-hot-cold zones. The substrate used for these experiments is kapton. (c) Temperature gradient curve is shown. T_{MAX} and ∇T_{MAX} are 210 and 27 °C/mm, respectively. (d) AFM morphology of the R2R CZA-S annealed 75 nm thick PS-PMMA thin film at the velocity of 25 μm/s. Size of scale bar is 200 nm.

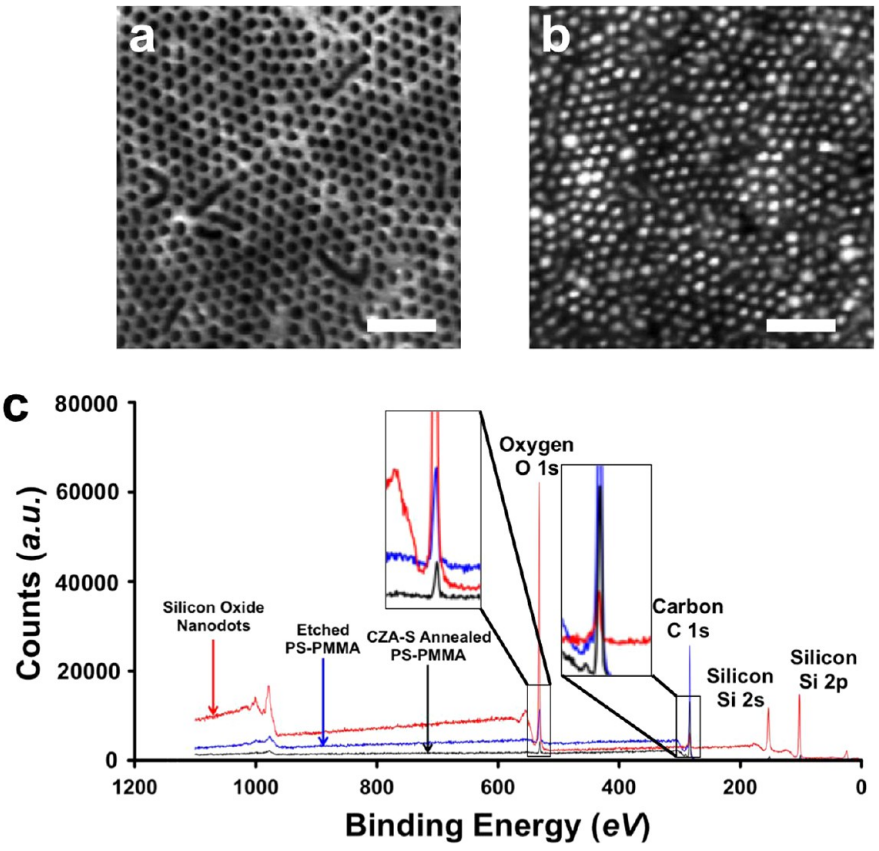

Figure 5. Fabrication of high-density silicon oxide nanodots. (a) Height image of the etched PS-PMMA BCP thin film. The PMMA phase is etched leaving behind a porous matrix. (b) Height image of the high-density silicon oxide nanodots fabricated from the etched PS-PMMA matrix. (c) X-ray photoelectron spectra (XPS) of PS-PMMA thin films after CZA-S annealing, after etching and after fabrication of silicon oxide nanodots. Size of scale bar is 200 nm.

The resulting temperature gradient profile is shown in Figure 4c. The T_{MAX} and ∇T_{MAX} are 210 and 27 °C/mm, respectively. The CZA-S annealing velocity is maintained at 25 μm/s with a T_g to T_g residence time of *ca.* 10 min. We perform grazing incidence small-angle X-ray scattering (GISAXS) measurements to determine the through-film thickness structure over the entire film-width (refer to Supporting Information Figure S5).[52] The GISAXS measurement is taken at an incident angle of 0.3° that is much larger than polymer critical angle (*ca.* 0.11−0.12°). This ensures that the X-rays illuminate the entire film and the GISAXS results indicate the through film morphology. The absence of scattering peaks in the q_z-direction of the GISAXS image (Supporting Information Figure S5) indicates that the nanostructure is uniform in the film normal direction.

We are currently performing *in situ* GISAXS measurements where we measure the BCP thin film morphology on smooth quartz substrates, while undergoing CZA-S annealing. Due to the smooth surface, we are able to observe out-of-plane oscillations (vertical cylinder form-factor) that are inversely proportional to the film thickness indicative of through film vertical morphology. By comparison, the GISAXS of an identical film processed differently that exhibits mixed morphology of vertical and horizontal cylinders (by AFM) is very different as shown in the Supporting Information Figure S6. The R2R CZA-S annealed PS-PMMA thin film was also imaged (Figure 4f) with AFM that revealed *ca.* 88% hexagonally well packed vertical population, in agreement with the CZA-S experiments of Figure 1. In principle, we have thus successfully demonstrated the rapid large-scale fabrication of vertically oriented block copolymer thin films that could further be used for a wide spectrum of applications. Another important observation based on the similarity of the BCP-DSA results on quartz *versus* kapton, Figure 1 and Figure 4, respectively, is that the self-assembly process is largely insensitive to the underlying substrate chemistry (quartz has a substrate surface energy of 70 mJ/m^2 where as kapton has a substrate surface energy of 42 mJ/m^2) in the limit of optimum CZA-S annealing velocities for PS-PMMA thin films.

Finally, we demonstrate that the vertically oriented BCP thin films obtained *via* CZA-S annealing can be used as functional templates. We observe good pattern transfer only for PS-PMMA films that are annealed at the optimized CZA-S conditions (see Supporting Information Figure S7 for examples of imperfect pattern transfer). For the purpose of demonstrating their functional nature, we fabricate high-density arrays of silicon oxide nanodots employing a well-known

block-copolymer templating method that has been developed by Russell *et al.*[53] The PS-PMMA thin films that were CZA-S annealed at 15 μm/s are ultraviolet (UV)-etched to selectively degrade and remove the PMMA phase while cross-linking the PS phase. The etched film morphology is shown in Figure 5a (height image) and shows excellent correlation with the pre-etched morphology (Figure 1h). The etched films were then spin-coated with 0.1% w/w solution of low molecular weight polydimethylsiloxane (PDMS) oil (Thermal C10, Julabo USA, Inc.) in heptane followed by thermal annealing at 90 °C for 2 h. The nanopores exert a capillary force on the PDMS oil causing the PDMS oil to be driven in to the pores. After the 2 h of thermal annealing, the thin films are exposed to ozone forming high energy UV light. This causes densification of the PDMS oil, *i.e.*, ozone causes dissociation of PDMS methyl groups and formation of Si−O−Si bonds, and at the same time also degrades the PS matrix.[54]

Figure 5b shows the AFM height image of the high-density array silicon oxide nanodots (notice the conversion of black holes in Figure 5a into white dots in Figure 5b) with an areal density of 5.45×10^{10} nanodots/cm^2. Figure 5c shows the X-ray photoelectron spectroscopy (XPS) measurements of CZA-S annealed PS-PMMA thin film, etched thin film and thin film converted to silicon oxide nanodots arrays. The transformation in chemical composition as the thin film is etched and converted to silicon oxide nanodots can be all clearly observed in the XPS data. The etching process causes slight oxidation of the PS groups that causes the increase in the oxygen content in the etched film as compared to the pre-etched film. The silicon oxide nanodot formation process leads to almost complete removal of the carbon containing groups as seen by the negligible carbon content. The oxygen and silicon content on the other hand increases dramatically as seen by the sharp O 1s, Si 2s and Si 2p peaks in Figure 5 c. This proves that the block copolymer template has been completely etched and converted to silicon oxide nanodots array.

CONCLUSION

We have demonstrated that CZA-S is a novel dynamic thermal annealing technique that can be used to continuously and rapidly fabricate vertically oriented block copolymer thin films on rigid and flexible substrates. These vertically oriented nanostructures can further be used for a wide spectrum of applications as demonstrated by the conversion of the vertical cylinders into high-density (5.45×10^{10}/cm^2) silicon oxide nanodots. We have, for the first time, quantitatively compared the advantages of the dynamic CZA-S process over the static conventional oven thermal annealing process. Most importantly, we also report, for the first time, successful scale-up of the CZA-S process on a prototype custom-built 70 ft × 1 ft R2R machine with nine consecutive CZA units that is important for commercializing oriented block copolymer thin films.

METHODS

Thin film samples of poly(styrene-*block*-methylmethacrylate) (PS-PMMA) di-block copolymer were used in these studies. PS-PMMA, total molar mass 82 kg/mol (57−25 kg/mol, PDI ~ 1.07) was purchased from Polymer Source, Inc. and used as obtained. The BCP thin film morphology is sensitive to PDI; we have obtained reproducible results up to PDI of 1.2. The %PS residual homopolymer in the block copolymers from Polymer Source was less than 5% w/w. BCP thin films were coated on ultraviolet, ozone cleaned quartz substrates that were obtained from G.M. Associates, Inc. Thickness of these thin films was ≈75 nm as measured by a UV−vis interferometer (F-20 UV by Filmetrics, Inc.). The BCP samples were dried at 60 °C for 24 h under vacuum before the annealing process. The detailed procedure for the CZA-S experiments is explained in detail in our recent papers.[38−40] The dynamic thermal gradient approach is based on the original hot-wire design concept by Lovinger *et al.* for directional crystallization of semi-crystalline polymers.[42] The width of the hot wire with ceramic encapsulation that is used for lab-scale CZA-S experiments is 3 mm. The maximum temperature (T_{MAX}) of the temperature gradient during zone annealing is 210 °C and the maximum temperature gradient (∇T) thus developed is 45 °C/mm. For TEM characterization, the quartz substrates were precoated with a thin layer (<10 nm) of poly(4-styrenesulfonic acid) (PSS, Sigma Aldrich) and heated at 160 °C for 12 h.[55] PSS coated quartz substrates were then UVO treated for 30 min to make them hydrophilic. These substrates were then coated with PS-PMMA thin films and CZA-S annealed, followed by which they were immersed in distilled water to dissolve the PSS layer causing the CZA-S annealed PS-PMMA thin films to float in water. The floating PS-PMMA films were then transferred onto copper TEM grids, dried and imaged using a JEOL JEM-1230 Transmission Electron Microscope (TEM) operated at 200 kV. The image analysis procedure for calculating the %vertical cylinder population is given in the Supporting Information Figure S8. For R2R CZA-S experiments, the substrate used was the low thermal conductivity flexible Kapton (Type VN, Dupont) film, with a thickness of 125 μm. The width of the hot zone for R2R CZA-S experiments was 10 mm. The BCP thin films were subjected to a T_{MAX} of 210 °C with a ∇T_{MAX} of about 27 °C/mm. The sample translation rate was set at 25 μm/s, which led to a T_g to T_g residence time of *ca.* 10 min. GISAXS measurements were performed at the X9 beamline of the National Synchrotron Light Source (NSLS) at Brookhaven National Laboratory. An incident X-ray beam of 13.5 keV (wavelength = 0.0918 nm) energy was used and samples were measured under vacuum (~40 Pa). GISAXS experiments were performed at incidence angles above the film-vacuum critical angle, with data collected using a charged-coupled device (CCD) detector. Data conversion to *q*-space was accomplished using Silver Behenate powder as a standard. The process for converting the etched BCP template to silicon oxide nanodots arrays is adopted from Russell *et al.* and is explained in detail in their recent publication.[48] X-ray photoelectron spectroscopy (XPS) survey scans were obtained using a PHI 5000 VersaProbe II Scanning XPS Microprobe with a monochromatic Al Kα source (1486.6 eV) operating at 25 W. The pass energy and the step size were 117.4 and 0.5 eV, respectively. Pressure was maintained below 10^{-6} Pa during XPS analysis.

Conflict of Interest: The authors declare no competing financial interest.

Supporting Information Available: AFM images of the PS-PMMA thin films that CZA-S annealed and thermally annealed in a vacuum oven for different time periods, the image analysis method to analyze the %vertical cylinder population, GISAXS measurement of R2R CZA-S annealed and oven annealed PS-PMMA thin films, imperfect pattern transfer of silicon oxide nanodot arrays and AFM images of CZA-S annealed PS-P2VP thin film. This material is available free of charge *via* the Internet at http://pubs.acs.org.

Acknowledgment. G.S. and A.K. would like to thank Prof. Bryan Vogt, Dr. Diya Bandhyopadhyay and Yan Luo for fruitful discussions. This CZA-S research work was entirely supported by the National Science Foundation (NSF), Division of Materials Research (DMR), Collaborative Grant NSF DMR-1006421. Supporting GISAXS was carried out at the National Synchrotron Light Source, and the Center for Functional Nanomaterials, Brookhaven National Laboratory, which is supported by the U.S. Department of Energy, Office of Basic Energy Sciences, under Contract No. DE-AC02-98CH10886. The Third Frontier Program of State of Ohio provided the funding for the R2R manufacturing line.

REFERENCES AND NOTES

1. Fasolka, M. J.; Mayes, A. M. Block Copolymer Thin Films: Physics and Applications. *Annu. Rev. Mater. Res.* **2001**, *31*, 323–355.
2. Bates, F. S.; Fredrickson, G. H. Block Copolymer Thermodynamics: Theory and Experiment. *Annu. Rev. Phys. Chem.* **1990**, *41*, 527–557.
3. Hamley, I. W. Ordering in Thin Films of Block Copolymers: Fundamentals to Potential Applications. *Prog. Polym. Sci.* **2009**, *34*, 1161–1210.
4. Darling, S. B. Directing the Self Assembly of Block Copolymers. *Prog. Polym. Sci.* **2007**, *32*, 1152–1204.
5. Marencic, A. P.; Register, R. A. Controlling Order in Block Copolymer Thin Films for Nanopatterning Applications. *Annu. Rev. Chem. Biomol. Eng.* **2010**, *1*, 277–297.
6. Segalman, R. A. Patterning with Block Copolymer Thin Films. *Mater. Sci. Eng., R* **2005**, *48*, 191–226.
7. Kim, H.-C.; Park, S.-M.; Hinsberg, W. D. Block Copolymer Based Nanostructures: Materials, Processes, and Applications to Electronics. *Chem. Rev.* **2010**, *110*, 146–177.
8. Cheng, J. Y.; Mayes, A. M.; Ross, C. A. Nanostructure Engineering by Templated Self-Assembly of Block Copolymers. *Nat. Mater.* **2004**, *3*, 823–828.
9. Park, M.; Harrison, C.; Chaikin, P. M.; Register, R. A.; Adamson, D. H. Block Copolymer Lithography: Periodic Arrays of 10^{11} Holes in 1 Square Centimeter. *Science* **1997**, *276*, 1401–1404.
10. Cheng, J. Y.; Ross, C. A.; Chan, V. Z.; Thomas, E. L.; Lammertink, R. G. H.; Vancso, G. J. Formation of a Cobalt Magnetic Dot Array *via* Block Copolymer Lithography. *Adv. Mater.* **2001**, 1174–1178.
11. Hawker, C.; Russell, T. Block Copolymer Lithography: Merging "Bottom- Up" with "Top- Down" Processes. *MRS Bull.* **2005**, *30*, 952–966.
12. Lim, H. S.; Lee, J.-H.; Walish, J. J.; Thomas, E. L. Dynamic Swelling of Tunable Full-Color Block Copolymer Photonic Gels *via* Counterion Exchange. *ACS Nano* **2012**, *6*, 8933–8939.
13. Urbas, A. M.; Maldovan, M.; DeRege, P.; Thomas, E. L. Bicontinuous Cubic Block Copolymer Photonic Crystals. *Adv. Mater.* **2002**, *14*, 1850–1853.
14. Mistark, P.; Park, S.; Yalcin, S.; Lee, D. Block-Copolymer-Based Plasmonic Nanostructures. *ACS Nano* **2009**, *3*, 3987–3992.
15. Shin, D. O.; Jeong, J.-R.; Han, T. H.; Koo, C. M.; Park, H.-J.; Lim, Y. T.; Kim, S. O. A Plasmonic Biosensor Array by Block Copolymer Lithography. *J. Mater. Chem.* **2010**, *20*, 7241–7247.
16. Jung, Y. S.; Jung, W.; Tuller, H. L.; Ross, C. A. Nanowire Conductive Polymer Gas Sensor Patterned Using Self-Assembled Block Copolymer Lithography. *Nano Lett.* **2008**, *8*, 3776–3780.
17. Ross, C. A. Patterned Magnetic Recording Media. *Annu. Rev. Mater. Res.* **2001**, *2*, 203–235.
18. Phillip, W. A.; O'Neill, B.; Rodwogin, M.; Hillmyer, M. A.; Cussler, E. L. Self-Assembled Block Copolymer Thin Films as Water Filtration Membranes. *ACS Appl. Mater. Interfaces* **2010**, *2*, 847–853.
19. Rösler, A.; Vandermeulen, G. W. M.; Klok, H.-A. Advanced Drug Delivery Devices *via* Self-Assembly of Amphiphilic Block Copolymers. *Adv. Drug Delivery Rev.* **2012**, *64*, 270–279.
20. Shimomura, M.; Sawadaishi, T. Bottom-up Strategy of Materials Fabrication: A New Trend in Nanotechnology of Soft Materials. *Curr. Opin. Colloid Interface Sci.* **2001**, *6*, 11–16.
21. Meng, Y.; Gu, D.; Zhang, F.; Shi, Y.; Yang, H.; Li, Z.; Yu, C.; Tu, B.; Zhao, D. Ordered Mesoporous Polymers and Homologous Carbon Frameworks: Amphiphilic Surfactant Templating and Direct Transformation. *Angew. Chem.* **2005**, *117*, 7215–7221.
22. Kimura, M.; Misner, M. J.; Xu, T.; Kim, S. H.; Russell, T. P. Long-Range Ordering of Diblock Copolymers Induced by Droplet Pinning. *Langmuir* **2003**, *19*, 9910–9913.
23. Hong, S. W.; Voronov, D. L.; Lee, D. H.; Hexemer, A.; Padmore, H. A.; Xu, T.; Russell, T. P. Controlled Orientation of Block Copolymers on Defect-free Faceted Surfaces. *Adv. Mater.* **2012**, *24*, 4278–83.
24. Park, S.; Lee, D. H.; Xu, J.; Kim, B.; Hong, S. W.; Jeong, U.; Xu, T.; Russell, T. P. Square-Inch Arrays from Block Copolymers with Lateral Order. *Science* **2009**, 1030–1033.
25. Woo, S.; Huh, J.; Gu, X.; Hyun, D.; Ho, W.; Park, S.; Xu, T. Unidirectionally Aligned Line Patterns Driven by Entropic Effects on Faceted Surfaces. *Proc. Natl. Acad. Sci. U.S.A.* **2012**, *109*, 1402–1406.
26. Bita, I.; Yang, J. K. W.; Jung, Y. S.; Ross, C. A.; Thomas, E. L.; Berggren, K. K. Graphoepitaxy of Self-Assembled Block Copolymers on Two-Dimensional Periodic Patterned Templates. *Science* **2008**, *321*, 939–943.
27. Kim, S. O.; Solak, H. H.; Stoykovich, M. P.; Ferrier, N. J.; Pablo, J. J. De; Nealey, P. F. Epitaxial Self-Assembly of Block Copolymers on Lithographically Defined Nanopatterned Substrates. *Nature* **2003**, *424*, 411–414.
28. Ruiz, R.; Kang, H.; Detcheverry, F. A.; Dobisz, E.; Kercher, D. S.; Albrecht, T. R.; Pablo, J. J. de; Nealey, P. F. Density Multiplication and Improved Lithography by Directed Block Copolymer Assembly. *Science* **2008**, *321*, 936–939.
29. Zhang, X.; Harris, K. D.; Wu, N. L. Y.; Murphy, J. N.; Buriak, J. M. Fast Assembly of Ordered Block Copolymer Nanostructures through Microwave Annealing. *ACS Nano* **2010**, *4*, 7021–7029.
30. Park, W. I.; Kim, K.; Jang, H.-I.; Jeong, J. W.; Kim, J. M.; Choi, J.; Park, J. H.; Jung, Y. S. Directed Self-Assembly with Sub-100 Degrees Celsius Processing Temperature, Sub-10 Nanometer Resolution, and Sub-1 minute Assembly Time. *Small* **2012**, *8*, 1563–1569.
31. Bates, C. M.; Seshimo, T.; Maher, M. J.; Durand, W. J.; Cushen, J. D.; Dean, L. M.; Blachut, G.; Ellison, C. J.; Willson, C. G. Polarity-Switching Top Coats Enable Orientation of Sub-10-nm Block Copolymer Domains. *Science* **2012**, *338*, 775–779.
32. Han, W.; He, M.; Byun, M.; Li, B.; Lin, Z. Large-Scale Hierarchically Structured Conjugated Polymer Assemblies with Enhanced Electrical Conductivity. *Angew. Chem.* **2013**, *52*, 2564–2568.
33. Son, J. G.; Gotrik, K. W.; Ross, C. A. High-Aspect-Ratio Perpendicular Orientation of PS-*b*-PDMS Thin Films under Solvent Annealing. *ACS Macro Lett.* **2012**, *1*, 1279–1284.
34. Borah, D.; Shaw, M. T.; Holmes, J. D.; Morris, M. A. Sub-10 nm Feature Size PS-*b*-PDMS Block Copolymer Structures Fabricated by a Microwave Assisted Solvothermal Process. *ACS Appl. Mater. Interfaces* **2013**, *5*, 2004–2012.
35. Bodycomb, J.; Funaki, Y.; Kimishima, K.; Hashimoto, T. Single-Grain Lamellar Microdomain from a Diblock Copolymer. *Macromolecules* **1999**, *32*, 2075–2077.

36. Angelescu, D. E.; Waller, J. H.; Adamson, D. H.; Register, R. A.; Chaikin, P. M. Enhanced Order of Block Copolymer Cylinders in Single-Layer Films Using a Sweeping Solidification Front. *Adv. Mater.* **2007**, *19*, 2687–2690.
37. Yager, K. G.; Fredin, N. J.; Zhang, X.; Berry, B. C.; Karim, A.; Jones, R. L. Evolution of Block-copolymer Order through a Moving Thermal Zone. *Soft Matter* **2010**, *6*, 92–99.
38. Berry, B. C.; Bosse, A. W.; Douglas, J. F.; Jones, R. L.; Karim, A. Orientational Order in Block Copolymer Films Zone Annealed below the Order−Disorder Transition Temperature. *Nano Lett.* **2007**, *7*, 2789–2794.
39. Singh, G.; Yager, K. G.; Smilgies, D.-M.; Kulkarni, M. M.; Bucknall, D. G.; Karim, A. Tuning Molecular Relaxation for Vertical Orientation in Cylindrical Block Copolymer Films *via* Sharp Dynamic Zone Annealing. *Macromolecules* **2012**, *45*, 7107–7117.
40. Singh, G.; Yager, K. G.; Berry, B.; Kim, H.-C.; Karim, A. Dynamic Thermal Field-Induced Gradient Soft-Shear for Highly Oriented Block Copolymer Thin Films. *ACS Nano* **2012**, *6*, 10335–10342.
41. Pfann, W. G. Zone Melting. *Science* **1962**, *135*, 1101–1109.
42. Lovinger, A. J.; Chua, J. O.; Gryte, C. C. Studies on the α and β Forms of Isotactic Polypropylene by Crystallization in a Temperature Gradient. *J. Polym. Sci., Polym. Phys. Ed.* **1977**, *15*, 641–656.
43. Mita, K.; Tanaka, H.; Saijo, K.; Takenaka, M.; Hashimoto, T. Macroscopically Oriented Lamellar Microdomains Created by "Cold Zone-Heating" Method Involving OOT. *Polymer* **2008**, *49*, 5146–5157.
44. Iyoda, T.; Kamata, K.; Watanabe, R.; Komura, M.; Ochiai, H. Roll-to-Roll Processable PEO-LC Block Copolymer Template Films with Normally Oriented Nanocylinder Array Structures. In *Microprocesses and Nanotechnology, 2007 Digest of Papers*; Japan Society ofApplied Physics: Tokyo, Japan, 2007; pp 460−461. DOI: 10.1109/IMNC.2007.4456303.
45. Stafford, C. M.; Roskov, K. E.; Epps, T. H.; Fasolka, M. J. Generating Thickness Gradients of Thin Polymer Films *via* Flow Coating. *Rev. Sci. Instrum.* **2006**, *77*, 023908.
46. Kim, H.; Russell, T. Ordering in Thin Films of Asymmetric Diblock Copolymers. *J. Polym. Sci. Part B: Polym. Phys.* **2001**, *39*, 663–668.
47. Beaucage, G.; Banach, M. Relaxation of Polymer Thin Films in Isothermal Temperature-Jump Measurements. *J. Polym. Sci., Part B: Polym. Phys.* **2000**, *38*, 2929–2936.
48. Gu, X.; Liu, Z.; Gunkel, I.; Chourou, S. T.; Hong, S. W.; Olynick, D. L.; Russell, T. P. High Aspect Ratio Sub-15 nm Silicon Trenches from Block Copolymer Templates. *Adv. Mater.* **2012**, *24*, 5688–5694.
49. Roth, C. B.; McNerny, K. L.; Jagger, W. F.; Torkelson, J. F. Eliminating the Enhanced Mobility at the Free Surface of Polystyrene: Fluorescence Studies of the Glass Transition Temperature in Thin Bilayer Films of Immiscible Polymers. *Macromolecules* **2007**, *40*, 2568–2574.
50. Olayo-Valles, R.; Guo, S.; Lund, M. S.; Leighon, C.; Hillmyer, M. A. Perpendicular Domain Orientation in Thin Films of Polystyrene-Polylactide Diblock Copolymers. *Macromolecules* **2005**, *38*, 10101–10108.
51. Cakmak, M. Electromagnetic Processing Line. US Patent App US 2012/0135156 A1, July 14, 2010.
52. Vu, T.; Mahadevapuram, N.; Perera, G. M.; Stein, G. E. Controlling Domain Orientations in Thin Films of AB and ABA Block Copolymers. *Macromolecules* **2011**, *44*, 6121–6127.
53. Park, S.; Kim, B.; Wang, J.-Y.; Russell, T. P. Fabrication of Highly Ordered Silicon Oxide Dots and Stripes from Block Copolymer Thin Films. *Adv. Mater.* **2008**, *20*, 681–685.
54. Xue, C.-Y.; Zhang, W.; Choo, W. H. S.; Yang, K.-L. Simplest Method for Creating Micropatterned Nanostructures on PDMS with UV Light. *Langmuir* **2011**, *27*, 13410–13414.
55. Torres, J. M.; Wang, C. Q.; Coughlin, E. B.; Bishop, J. P.; Register, R. A.; Riggleman, R. A.; Stafford, C. M.; Vogt, B. D. Influence of chain stiffness on thermal and mechanical properties of polymer thin films. *Macromolecules* **2011**, *44*, 9040–9045.